Alexandria Engineering Journal (2016) 55, 275–285

HOSTED BY

Alexandria University

Alexandria Engineering Journal

www.elsevier.com/locate/aej
www.sciencedirect.com

Single walled carbon nanotubes on MHD unsteady flow over a porous wedge with thermal radiation with variable stream conditions

R. Kandasamy *, **I. Muhaimin, Radiah Mohammad**

Research Centre for Computational Mathematics, FSTPi, Universiti Tun Hussein Onn Malaysia, Johor 86400, Malaysia

Received 10 June 2015; revised 6 October 2015; accepted 28 October 2015
Available online 18 November 2015

KEYWORDS

Single walled carbon nanotubes;
Porous wedge;
Unsteady Hiemenz flow;
Thermal stratification;
Solar energy radiation

Abstract The objective of the present work was to investigate theoretically the effect of single walled carbon nanotubes (SWCNTs) in the presence of water and seawater with variable stream condition due to solar radiation energy. The conclusion is drawn that the flow motion and the temperature field for SWCNTs in the presence of base fluid are significantly influenced by magnetic field, convective radiation and thermal stratification. Thermal boundary layer of SWCNTs-water is compared to that of Cu-water, absorbs the incident solar radiation and transits it to the working fluid by convection.

1. Introduction

The thermal conductivity of heat transfer fluid plays an important role in the development of energy-efficient heat transfer equipment including electronics, HVAC&R, and transportation. Development of advanced heat transfer fluids is clearly essential to improve the effective heat transfer behavior of conventional heat transfer fluids. Nanomaterials have been extensively researched in recent years. Emerging nanotechnology shows promise in every aspect of engineering applications. Recently, there has been interest in using nanomaterials as additives to modify heat transfer fluids to improve their performance. The new class of heat transfer fluid is termed nanofluids which are formed by combining nanomaterials with heat transfer fluids. Dispersion or suspension of nanomaterials of high thermal conductivities into base fluids gives rise to higher thermal conductivity of the mixtures thereby increasing the heat transfer coefficient. Compared with millimeter- or micrometer-sized particle suspensions, nanofluids possess better long-term stability and rheological properties, and can have dramatically higher thermal conductivities.

Nanotubes are members of the fullerene structural family and it is adopted from their long, hollow structure with the walls designed by one-atom-thick sheets of carbon, called graphene. Carbon nanotubes are classified as single-walled carbon nanotubes (SWCNTs) and multi-walled carbon nanotubes (MWCNTs). Individual nanotubes naturally align themselves into "ropes" held together by van der Waals forces, more specifically, pi-stacking. Nanofluids have been designed for applications as advanced heat transfer fluids. A wide range of industrial processes associate with the transfer of heat energy and it has become a major assignment for industrial necessity. In this study, thermal conductivity enhancements of water in the presence of single-walled carbon nanotubes (SWCNTs) are presented. The thermal conductivities of

* Corresponding author. Tel.: +60 7 453 7416.
E-mail address: future990@gmail.com (R. Kandasamy).
Peer review under responsibility of Faculty of Engineering, Alexandria University.

http://dx.doi.org/10.1016/j.aej.2015.10.006

Nomenclature

B_0 magnetic flux density, kg s^{-2} A^{-1}
C_T temperature ratio, K
c_p specific heat at constant pressure, J kg^{-1} K^{-1}
g acceleration due to gravity, ms^{-2}
k_1 rate of chemical reaction, mol m^{-1} s^{-1}
k^* mass absorption coefficient, m^{-1}
K permeability of the porous medium, m^2
k_f thermal conductivity of the base fluid, kg m s^{-3} K^{-1}
k_s thermal conductivity of the nanoparticle, kg m s^{-3} K^{-1}
k_{nf} effective thermal conductivity of the nanofluid, kg m s^{-3} K^{-1}
Pr Prandtl number, $\frac{\nu_f}{\alpha_f}\left(\frac{\mathrm{m^2\ s^{-1}}}{\mathrm{m^2\ s^{-1}}}\right)$, –
Gr Grashof number, $\frac{g(\beta)_f \Delta T\ x^3}{\nu_f^2}\left(\frac{\mathrm{K^{-1}m\ s^{-2}K\ m^3}}{\mathrm{m^4\ s^{-2}}}\right)$, –
M magnetic parameter, $\frac{\sigma\ B_0^2 x}{U\ \rho_f}$, $\left(\frac{\Omega^{-1}\ \mathrm{m^{-1}}B_0^2\ \mathrm{m}}{\mathrm{m\ s^{-1}\ kg\ m^{-3}}}\right)$, –
Re Reynolds number, $\frac{U\ x}{\nu_f}\left(\frac{\mathrm{m\ s^{-1}\ m}}{\mathrm{m^2\ s^{-1}}}\right)$, –
q''_{rad} incident radiation flux of intensity, kg m^{-1} s^{-3} K^{-1}
Q_0 rate of source/sink, kg m^{-2}
t time, s
T temperature of the fluid, K
T_w temperature of the wall, K
T_∞ temperature of the fluid far away from the wall, K
N thermal radiation parameter, $\frac{16\sigma_1 T_w^3}{3k_f k^*} = \left(\frac{\mathrm{kg\ s^{-3}\ K^{-4}\ K^3}}{\mathrm{kg\ m\ s^{-3}\ K^{-1}\ m^{-1}}}\right)$, –
u, v velocity components in x and y direction, m s^{-1}
$U(x)$ flow velocity of the fluid away from the wedge, m s^{-1}
V_0 velocity of suction/ injection, m s^{-1}

Greek symbols
α_{nf} thermal diffusivity of the nanofluid, m^2 s^{-1}
β_f thermal expansion coefficients of the base fluid, K^{-1}
ρ_f density of the base fluid, kg m^{-3}
ρ_s density of the nanoparticle, kg m^{-3}
ρ_{nf} effective density of the nanofluid, kg m^{-3}
$(\rho\ c_p)_{nf}$ heat capacitance of the nanofluid, J m^{-3} K^{-1}
$(\rho\ \beta)_{nf}$ volumetric coefficient of thermal expansion of nanofluid, K^{-1}
σ electric conductivity, Ω^{-1} m^{-1}
σ_1 Stefan–Boltzmann constant, kg s^{-3} K^{-4}
μ_f dynamic viscosity of the base fluid, kg m^{-1} s^{-1}
μ_{nf} effective dynamic viscosity of the nanofluid, kg m^{-1} s^{-1}
ν_{nf} dynamic viscosity of the nanofluid, m^2 s^{-1}
δ time-dependent length scale, s
δ_1 heat source/sink parameter, $\frac{Q_0\ x}{(\rho\ c_p)_f\ U}$, $\left(\frac{\mathrm{kg\ m^{-1}\ s^{-3}\ K^{-1}\ m}}{\mathrm{kg\ m^{-2}\ s^{-1}(m^2\ s^{-2}\ K^{-1})}}\right)$, –
λ porous parameter, $\frac{\nu_f\ x}{K\ U}\left(\frac{\mathrm{m^2\ s^{-1}\ m}}{\mathrm{m\ m^2\ s^{-1}}}\right)$, –
Ω resistance, kg m^2 s^{-3} A^{-2}
ξ distance along the wedge, m
ζ nanoparticle volume fraction, –
ψ dimensionless stream function, –
η similarity variable, –
f dimensionless stream function, –
θ dimensionless stream function, –

nanofluids containing SWCNTs dispersed in the presence of base fluids are improved significantly compared to pure fluids. The SWCNTs dispersed in base fluid can form an extensive three-dimensional SWCNTs network that facilitates thermal transport. Developing issue in heat and mass transfer enhancement relies on the use of nanofluids [1,2]. Nanofluids consist of nanometer-sized particles with high thermal conductivity dispersed in a common base fluid such as water or engine oil. Due to their high thermal conductivity compared to base fluids and their performance in energy devices, nanofluids are interesting candidates for heat transfer enhancement in many fields and applications [3–7].

Several studies have been previously performed on the heat transfer enhancement of nanofluids flowing through a tube under laminar regime. It is well admitted that experimental convective heat transfer coefficients of nanofluids varied with increase of the flow velocity and volume fraction. These coefficients are far higher than the ones of base fluids under the same conditions, as reported in [8] for a wide variety of nanofluids containing Cu or Al_2O_3 spherical nanoparticles. Similar results are also summarized in [9] considering other nanoparticle natures. The authors mentioned in particular that the measured Nusselt numbers of nanofluids are higher than the ones of base fluids, and increase with higher Reynolds numbers. However, few works reported the heat transfer coefficient measurement of nanofluids containing nanotubes and carbon nanotubes in particular, while they have a high thermal conductivity [10–12]. Hence, the potential of water based single walled carbon nanotubes (SWCNTs-water) nanofluids for heat transfer enhancement in coaxial tube exchanger due to solar radiation under laminar flow regime is here investigated numerically. These nanofluids appear to have a very high thermal conductivity and may be able to meet the rising demand as an efficient heat transfer agent.

Scientists and engineers have started showing interest in the study of heat transfer characteristics of these nanofluids. But a clear picture about the heat transfer through these nanofluids is yet to emerge. Saleem et al. [13], Haq et al. [14], Waqar et al. [15], Khan et al. [16] and Haq et al. [17] reported the large convective heat transfer enhancement of aqueous CNT under laminar flow in comparison with water for both low Reynolds number and weight fraction in nanotubes. The enhancement in convective heat transfer appeared to be strongly dependant on nanoparticle concentration and aspect ratio, Reynolds number and axial position. Also, heat transfer coefficient increased with Reynolds number and the highest enhancement was observed at the entrance region of the tube. Solar energy is one of the best sources of renewable energy with minimal

environmental impact (Sharma et al. [18], Hunt [19], Buongiorno and Hu [20], Buongiorno [21], Kuznetsov and Nield [22], Nield and Kuznetsov [23] and Cheng–Minkowycz [24]). The researches, led by Lalwani et al. [25], Nield and Kuznetsov [26], Kuznetsov and Nield [27], Khan and Pop [28], Makinde and Aziz [29], Nadeem and Lee [30] and Khan et al. [31] found that their single-walled carbon nanotube (SWCNT) nanofluid exhibits an increase in conductivity of up to almost 15%; a value significantly higher than what has been achieved with nanoparticle-based nanofluids. SWCNT have unique electronic and mechanical properties which can be used in numerous applications, such as field-emission displays, nanocomposite materials, nanosensors, and logic elements. These materials are on the leading-edge of electronic fabrication, and are expected to play a major role in the next generation of heat transfer and miniaturized electronics.

The effect of magnetic field on convective flow along a porous wedge plate in thermally stratified nanofluids under the convective boundary condition has not been reported in the literature. Based on the above reasons, it could be stated that little published literature exists regarding SWCNTs in water and their applications as heat transfer fluid. Also, there is an inconsistency in the few reported studies on the convective heat behavior of CNT-nanofluids. Therefore, it was decided to study the convective heat transfer behavior of SWCNTs and copper nanoparticles in the presence of base fluid.

2. Mathematical analysis

Consider two-dimensional unsteady boundary layer flow of incompressible viscous nanofluids (water based copper nanoparticles and single walled carbon nanotubes) past a porous wedge sheet in the presence of solar energy radiation (see, Fig. 1). The temperature at the wedge surface takes the constant value T_w, while the ambient value, attained as y tends to infinity, takes the constant value T_∞. It is considered that the influence of a constant magnetic field of strength B_0 which is applied normally to the sheet. It is further assumed that the induced magnetic field is negligible in comparison with the applied magnetic field (as the magnetic Reynolds number is small). The porous medium is assumed to be transparent and in thermal equilibrium with the fluid. The thermal dispersion effect is minimal when the thermal diffusivity of the porous matrix is of the same order of magnitude as that of the working fluid. The non-reflecting absorbing ideally transparent wedge plate receives an incident radiation flux of intensity q''_{rad}. This radiation flux penetrates the plate and is absorbed in an adjacent fluid of absorption coefficient. The fluid is a water based nanofluid containing single walled carbon nanotubes. As mentioned before, the working fluid is assumed to have heat absorption properties. For the present application, the porous medium absorbs the incident solar radiation and transits it to the working fluid by convection. The thermophysical properties of the nanofluids are given in Table 1. Under the above assumptions, the boundary layer equations governing the flow and thermal field can be written in dimensional form as

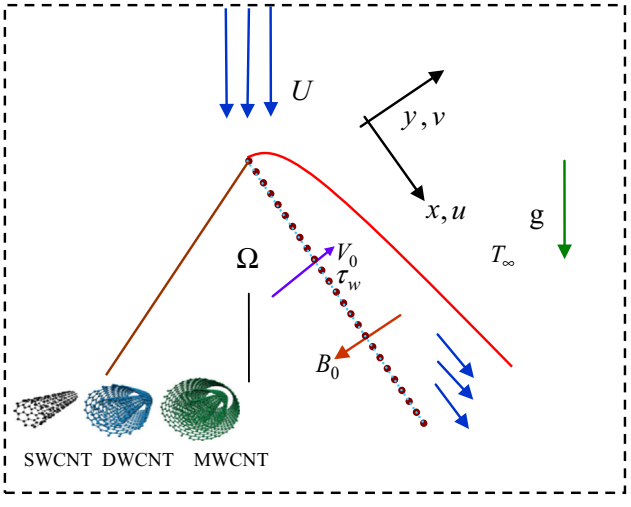

Figure 1 Physical flow model over a porous wedge sheet.

$$\frac{\partial \bar{u}}{\partial \bar{x}} + \frac{\partial \bar{v}}{\partial \bar{y}} = 0 \tag{1}$$

$$\frac{\partial \bar{u}}{\partial \bar{t}} + \bar{u}\frac{\partial \bar{u}}{\partial \bar{x}} + \bar{v}\frac{\partial \bar{u}}{\partial \bar{y}} = \frac{1}{\rho_{nf}}\left[\left(\frac{\partial U}{\partial t} + U\frac{dU}{dx}\right)\rho_{nf} + \mu_{f_n}\frac{\partial^2 \bar{u}}{\partial \bar{y}^2} + (\rho\beta)_{nf}\bar{g}(T - T_\infty)\cos\frac{\Omega}{2} - \left(\sigma B_0^2 + \frac{\nu_{nf}}{K}\rho_{nf}\right)(\bar{u} - U)\right] \tag{2}$$

$$\frac{\partial T}{\partial \bar{t}} + \bar{u}\frac{\partial T}{\partial \bar{x}} + \bar{v}\frac{\partial T}{\partial \bar{y}} = \frac{1}{(\rho\, c_p)_{nf}}\left(k_{nf}\frac{\partial^2 T}{\partial \bar{y}^2} - \frac{\partial q''_{rad}}{\partial y} - Q_0(T - T_\infty)\right) \tag{3}$$

The term $Q_0(T_\infty - T)$ is assumed to be the amount of heat source/ sink per unit volume and Q_0 is a constant. $q''_{rad} = -\frac{4\sigma_1}{3k^*}\frac{\partial T^4}{\partial y}$ where $T^4 \cong 4T_\infty^3 T - 3T_\infty^4, \sigma_1$ is the Stefan–Boltzmann constant and k^* is the mean absorption coefficient. In above expressions, u and v are the velocity components along the x-axis and y-axis, respectively, T is the temperature of the base fluid, ρ_{nf} is the density of nanofluid, μ_{nf} is the viscosity of nanofluid and α_{nf} is the thermal diffusivity of nanofluid [34] defined as,

$$\mu_{nf} = \frac{\mu_f}{(1-\varphi)^{2.5}}, \quad \alpha_{nf} = \frac{k_{nf}}{(\rho\, c_p)_{nf}}, \quad \nu_{nf} = \frac{\mu_{nf}}{\rho_{nf}},$$
$$\rho_{nf} = (1-\varphi)\rho_f + \varphi\rho_s (\rho\beta)_{nf} = (1-\varphi)(\rho\beta)_f + \varphi(\rho\beta)_s,$$
$$(\rho\, c_p)_{nf} = (1-\varphi)(\rho\, c_p)_f + \varphi(\rho\, c_p)_{CNT},$$
$$\frac{k_{nf}}{k_f} = \frac{1 - \varphi + 2\varphi\left(\frac{k_{CNT}}{k_{CNT}-k_f}\right)\ln\left(\frac{k_{CNT}+k_f}{2k_f}\right)}{1 - \varphi + 2\varphi\left(\frac{k_f}{k_{CNT}-k_f}\right)\ln\left(\frac{k_{CNT}+k_f}{2k_f}\right)} \tag{4}$$

μ_f is the viscosity of base fluid, φ is the nanoparticle fraction, $(\rho\, c_p)_{nf}$ is the effective heat capacity of a nanoparticles, k_{nf} is the thermal conductivity of nanofluid, k_f and k_s are the thermal conductivities of the base fluid and nanoparticles respectively while ρ_f and ρ_s are the thermal conductivities of the base fluid and nanoparticles respectively. The corresponding boundary conditions are stated as

$$\bar{u} = 0, \quad \bar{v} = -v_0, \quad T = T_w + c_1 x^{n_1} \text{ at } \bar{y} = 0; \quad \bar{u} \to U = \frac{\nu_f x^m}{\delta^{m+1}}, \quad T = T_\infty \text{ as } T \to T_\infty \tag{5}$$

where c_1 *and* n_1 (power index) are constants and v_0 and T_w are the suction (> 0) or injection (< 0) velocity and the fluid tem-

Table 1 Thermophysical properties of fluid and nanoparticles, Haq et al. [34] and Lynne et al. [35].

	ρ (kg/m^3)	c_p (J/kg K)	k (W/mK)	$\beta \times 10^{-5}$ (K^{-1})	$\alpha \times 10^{-7}$ (m^2/s)
Pure water	997.1	4179	0.613	21	1.47
Seawater	1021	3993	0.596	4.181	1.46
Copper (Cu)	8933	385	401	1.67	1163.1
Alumina (Al_2O_3)	3970	765	40	0.85	131.7
Titanium (TiO_2)	4250	6862	8.9538	0.9	30.7
SWCNTs	2600	425	6600	0.33	2.0

perature at the plate. Under this consideration, the potential flow velocity of the wedge can be written as $U(x,t) = \frac{v_f x^m}{\delta^{m+1}}$, $\beta_1 = \frac{2m}{1+m}$ whereas δ is the time-dependent length scale which is taken to be $\delta = \delta(t)$ and β_1 is the Hartree pressure gradient parameter that corresponds to $\beta_1 = \frac{\Omega}{\pi}$ for a total angle Ω of the wedge, the temperature of the fluid is assumed to vary a power-law function, T is the local temperature of the nanofluid, $\bar{g}$ is the acceleration due to gravity and K is the permeability of the porous medium.

Following the lines of Kafoussias and Nanousis [32], the changes of variables are

$$\eta = y\sqrt{\frac{(1+m)}{2}}\sqrt{\frac{x^{m-1}}{\delta^{m+1}}}, \quad \psi = \sqrt{\frac{2}{1+m}}\frac{v_f x^{\frac{m+1}{2}}}{\delta^{\frac{m+1}{2}}} f(\eta) \quad \text{and} \quad \theta = \frac{T - T_\infty}{T_w - T_\infty} \tag{6}$$

By introducing the stream function ψ, which defined as $u = \frac{\partial \psi}{\partial y}$ and $v = -\frac{\partial \psi}{\partial x}$, then the system of Eqs. (2) and (3) become

$$\frac{\partial^2\psi}{\partial t \partial y} + \frac{\partial \psi}{\partial y}\frac{\partial^2 \psi}{\partial x \partial y} - \frac{\partial \psi}{\partial x}\frac{\partial^2 \psi}{\partial y^2} = \frac{1}{(1-\zeta+\zeta\frac{\rho_s}{\rho_f})}\left[\left\{\left(1-\zeta+\zeta\frac{(\rho\beta)_s}{(\rho\beta)_f}\right) g(\rho\beta)_f \Delta T \sin\frac{\Omega}{2}\theta\right\} + \frac{v_f}{(1-\zeta)^{2.5}}\frac{\partial^3\psi}{\partial y^3} + U\frac{dU}{dx} - \left((1-\zeta)^{2.5}\frac{\sigma B_0^2}{\rho_{nf}} + \frac{v_{nf}}{K}\right)(u-U)\right] \tag{7}$$

$$\frac{\partial T}{\partial t} + \frac{\partial \psi}{\partial y}\frac{\partial T}{\partial x} - \frac{\partial \psi}{\partial x}\frac{\partial T}{\partial y} = \frac{1}{1-\zeta+\zeta\frac{(\rho\, c_p)_s}{(\rho\, c_p)_f}}\left[\frac{1}{Pr}\left\{\frac{k_{f_n}}{k_f}\frac{\partial^2 T}{\partial y^2} - \frac{4\sigma_1}{3k^*}\frac{\partial^2 T^4}{\partial y^2}\right\} - \frac{Q_0\,\Delta T}{(\rho\, c_p)_f}\theta\right] \tag{8}$$

with the boundary conditions

$$\frac{\partial \psi}{\partial y} = 0, \quad \frac{\partial \psi}{\partial x} = -V_0, \quad T = T_w \text{ at } y = 0; \quad \frac{\partial \psi}{\partial y} \to \frac{v\, x^m}{\delta^{m+1}}, \quad T = T_\infty \text{ as } \bar{y} \to \infty \tag{9}$$

The symmetry groups of Eqs. (7) and (8) are calculated using classical Lie group approach. The one-parameter infinitesimal Lie group of transformations leaving (7) and (8) invariant is defined as

$$x^* = x + \varepsilon\xi_1(x,y,\psi,\theta), \quad y^* = y + \varepsilon\xi_2(x,y,\psi,\theta), \quad \psi^* = \psi + \varepsilon\mu_1(x,y,\psi,\theta), \quad \theta^* = \theta + \varepsilon\mu_2(x,y,\psi,\theta) \tag{10}$$

From the algebraic technique, it is noticed that the form of infinitesimals is as

$$\xi_1 = c_1 x + c_2, \quad \xi_2 = g(x), \quad \mu_1 = c_3\psi + c_4 \quad \text{and} \quad \mu_2 = c_5\theta \tag{11}$$

where $g(x)$ is an arbitrary function.

Definitions of infinitesimal generators are

$$X_1 = x\frac{\partial}{\partial x} + g(x)\frac{\partial}{\partial y} + \psi\frac{\partial}{\partial \psi} + \theta\frac{\partial}{\partial \theta}, \quad X_2 = \frac{\partial}{\partial x} + g(x)\frac{\partial}{\partial y}, \quad X_3 = g(x)\frac{\partial}{\partial y} + \frac{\partial}{\partial \psi} \tag{12}$$

The partial differential equations governing the problem under consideration are transformed by a special form of Lie symmetry group transformations viz. one-parameter infinitesimal Lie group of transformation into a system of ordinary differential equations. For the present case, the generator X_1 with $g(x) = 0$ is taken. The characteristic equations are

$$\frac{dx}{x} = \frac{dy}{0} = \frac{d\psi}{\psi} = \frac{d\theta}{\theta} \tag{13}$$

Solving the above equations, we get

$$\eta = y, \quad \psi = x\, f(\eta) \quad \text{and} \quad \theta = x\,\theta(\eta) \quad \text{where } \eta = \eta(x,t) \tag{14}$$

With the help of these relations, (7) and (8) become

$$f''' + \left(1-\zeta+\zeta\frac{\rho_s}{\rho_f}\right)(1-\zeta)^{2.5}\xi^2[\lambda_v(-2+2f'+\eta f'') + ff'' + \frac{2m}{m+1}(1-f'^2)] + \frac{2}{m+1}\left[\left\{\left(1-\zeta+\zeta\frac{(\rho\,\beta)_s}{(\rho\,\beta)_f}\right)\right\} \times \xi^{\frac{1}{1-m}}(1-\zeta)^{2.5}\gamma\,\sin\frac{\Omega}{2}\theta - (M(1-\zeta)^{2.5}+\lambda)\,(f'-1)\right] + \left(1-\zeta+\zeta\frac{\rho_s}{\rho_f}\right)(1-\zeta)^{2.5}\frac{1-m}{1=m}\xi\frac{\partial f}{\partial \xi}\left(\frac{\partial f}{\partial \eta} - \frac{\partial^2 f}{\partial \eta^2}\right) = 0 \tag{15}$$

$$\theta''\left(1+\frac{k_f N}{k_{f_n}}\right) - Pr\left\{1-\zeta+\zeta\frac{(\rho\, c_p)_s}{(\rho\, c_p)_f}\right\}\frac{k_f}{k_{f_n}} \times \left[\frac{2n_1}{m+1}f'\theta - f\theta' + \lambda_v\eta\,\theta' + \frac{2}{1+m}\delta_1\,\theta + \frac{1-m}{1+m}\left\{\xi\frac{\partial\theta}{\partial\xi}\frac{\partial f}{\partial\eta} - \xi\frac{\partial f}{\partial\xi}\frac{\partial\theta}{\partial\eta}\right\}\right] = 0 \tag{16}$$

The boundary conditions take the following form:

$$\frac{\partial f}{\partial \eta}=0,\quad \frac{m+1}{2}f+\frac{1-m}{2}\xi\frac{\partial f}{\partial \xi}=-S,\quad \theta=1 \text{ at } \eta=0 \text{ and } \frac{\partial f}{\partial \eta}=1,\quad \theta\to 0 \text{ as } \eta\to\infty \tag{17}$$

where $Pr=\frac{\nu_{nf}}{\alpha_{nf}}$ is the Prandtl number, $\lambda=\frac{\nu_{nf}x}{U\,K}$ is the porous media parameter, $\delta_1=\frac{Q_0\,x}{(\rho\,c_p)_f\,U}$ is heat source/sink parameter, $\gamma=\frac{Gr}{Re^2}$ is the buoyancy parameter or convection parameter, $Gr=\frac{g(\rho\beta)_{nf}\Delta T\,x^3}{\nu_{nf}^2}$ is the Grashof number, $Re=\frac{U\,x}{\nu_{nf}}$ is the Reynolds number, $M=\frac{\sigma\,B_0^2 x}{U\,\rho_{nf}}$ is the magnetic parameter, and $N=\frac{16\sigma_1 T_w^3}{3k_f\,k^*}$ is the conductive radiation parameter. In the present study, it is assigned the value 0.1. It is worth mentioning that $\gamma>0$ aids the flow and $\gamma<0$ opposes the flow, while $\gamma=0$, i.e., (T_w-T_∞) represents the case of forced convection flow. On the other hand, if γ is of a significantly greater order of magnitude than one, then the buoyancy forces will be predominant. Hence, combined convective flow exists when $\gamma=O(1)$. S is the suction parameter if $S>0$ and injection if $S<0$ and $\xi=k\,x^{\frac{1-m}{2}}$ (Kafoussias and Nanousis [32]) is the dimensionless distance along the wedge ($\xi>0$). At the first level of truncation, the terms accompanied by $\xi\frac{\partial}{\partial\xi}$ are small. This is particularly true when ($\xi\ll 1$). Thus the terms with $\xi\frac{\partial}{\partial\xi}$ on the right-hand sides of Eqs. (15) and (16) are deleted to get the following system of equations:

$$f'''+\left(1-\zeta+\zeta\frac{\rho_s}{\rho_f}\right)(1-\zeta)^{2.5}[\lambda_v(-2+2f'+\eta f'')+ff''+\frac{2m}{m+1}(1-f'^2)]+\frac{2}{m+1}\left[\left\{\left(1-\zeta+\zeta\frac{(\rho\,\beta)_s}{(\rho\,\beta)_f}\right)\right\}\times(1-\zeta)^{2.5}\gamma\cos\frac{\Omega}{2}\theta-(M(1-\zeta)^{2.5}+\lambda)\,(f'-1)\right]=0 \tag{18}$$

$$\theta''\left(1+\frac{k_f N}{k_{f_n}}\right)-Pr\left\{1-\zeta+\zeta\frac{(\rho\,c_p)_s}{(\rho\,c_p)_f}\right\}\frac{k_f}{k_{f_n}}\left[\frac{2n_1}{m+1}f'\theta-f\theta'+\lambda_v\,\eta\,\theta'+\frac{2}{1+m}\delta_1\,\theta\right]=0 \tag{19}$$

The boundary conditions take the following form:

$$f'=0,\quad f=-\frac{2S}{m+1},\quad \theta=1 \text{ at } \eta=0 \text{ and } f'=1,\quad \theta\to 0 \text{ as } \eta\to\infty \tag{20}$$

Further, we suppose that $\lambda_v=\frac{c}{x^{m-1}}$ where c is a constant so that $c=\frac{\delta^m}{\nu_f}\frac{\partial\delta}{\partial t}$ and integrating, it is obtained that $\delta=\left[c(m+1)\nu_f\,t\right]^{\frac{1}{m+1}}$. When $c=2$ and $m=1$ in δ and we get $\delta=2\sqrt{\nu_f\,t}$ which shows that the parameter δ can be compared with the well established scaling parameter for the unsteady boundary layer problems [33].

For practical purposes, the functions $f(\eta)$ and $\theta(\eta)$ allow us to determine the skin friction coefficient

$$C_f=\frac{\mu_{f_n}}{\rho_f U^2}\left(\frac{\partial u}{\partial y}\right)_{at\ y=0}=-\frac{1}{(1-\zeta)^{2.5}}(Rex)^{-\frac{1}{2}}f''(0) \tag{21}$$

and the Nusselt number

$$Nu_x=\frac{xk_{f_n}}{k_f(T_w-T_\infty)}\left(\frac{\partial T}{\partial y}\right)_{at\ y=0}=-(Re\ x)^{\frac{1}{2}}\frac{k_{f_n}}{k_f}\theta'(0) \tag{22}$$

respectively. Here, $Re_x=\frac{U\,x}{\nu_f}$ is the local Reynolds number.

3. Numerical solution

Eqs. (18) and (19) subjected to the boundary condition (20) are converted into the following simultaneous system of first order differential equations as follows:

$$f'(\eta)=u(\eta) \tag{23}$$

$$u'f(\eta)=v(\eta) \tag{24}$$

$$v'(\eta)=-A_1\left[\lambda_v-2+2u(\eta)+\eta\,v(\eta)+f(\eta)\,v(\eta)+\frac{2m}{m+1}(1-u(\eta)^2)\right]-\frac{2}{m+1}\left[A_2\gamma\cos\frac{\Omega}{2}\theta-(MA_3+\lambda)\,(u(\eta)-1)\right] \tag{25}$$

$$\theta'(\eta)=p(\eta) \tag{26}$$

$$A_1=\left(1-\zeta+\zeta\frac{\rho_{CNT}}{\rho_f}\right)(1-\zeta)^{2.5},\quad A_2=\left(1-\zeta+\zeta\frac{(\rho\,\beta)_{CNT}}{(\rho\,\beta)_f}\right)(1-\zeta)^{2.5},\quad A_3=(1-\zeta)^{2.5}$$

$$A_4=\left\{1-\zeta+\zeta\frac{(\rho\,c_p)_{CNT}}{(\rho\,c_p)_f}\right\},\quad A_5=\frac{1}{A6},\quad A_6=\left(1+\frac{k_f}{k_{f_n}}N\right)$$

$$p'(\eta)=Pr\frac{A_5}{A_6}A_4\frac{k_f}{k_{f_n}}\left[\frac{2n_1}{m+1}\theta(\eta)\,u(\eta)-f(\eta)p(\eta)+\lambda_v\,\eta\,p(\eta)+\frac{2}{1+m}\delta_1\,\theta(\eta)\right] \tag{27}$$

The initial conditions are

$$f(0)=-\frac{2S}{m+1},\quad u(0)=0,\quad v(0)=\alpha,\quad \theta(0)=1,\quad p(0)=\beta \tag{28}$$

where α and β are priori unknowns to be determined as a part of the solution.

By using DSolve subroutine in MAPLE we can get a solution for the system of Eqs. (23)–(27) with conditions (28). This software uses a fourth-fifth order Runge–Kutta–Fehlberg method as default to solve the boundary value problems numerically using the Dsolve command. The values of α and β are determined upon solving the boundary conditions $v(0)=\alpha$, and $p(0)=\beta$. Once α and β are determined, the system will be closed and can be solved numerically again by DSolve subroutine to get the final results. Consequently, only one integration path is enough to solve the problem instead of consuming the time with iteration techniques such as the shooting method. The numerical results are represented in the form of the dimensionless velocity and temperature in the presence of SWCNT – water and Cu-water.

Table 2 Comparison of skin friction coefficient $f''(0)$ for various values of M.

ζ	Rizwan et al. [34]		Present work	
	$\beta = 0.5$		$\beta = 0.5$	
	$M = 0$	$M = 0.5$	$M = 0$	$M = 0.5$
SWCNTs-water				
0.0	0.5912	0.6495	0.591178452	0.649493428
0.1	0.6680	0.7242	0.667965268	0.724248769
0.2	0.7504	0.8051	0.750374192	0.805072871
MWCNTs-water				
0.0	0.5912	0.6495	0.591194527	0.649522965
0.1	0.6508	0.7106	0.650793523	0.710573241
0.2	0.7180	0.7795	0.717956234	0.779531892

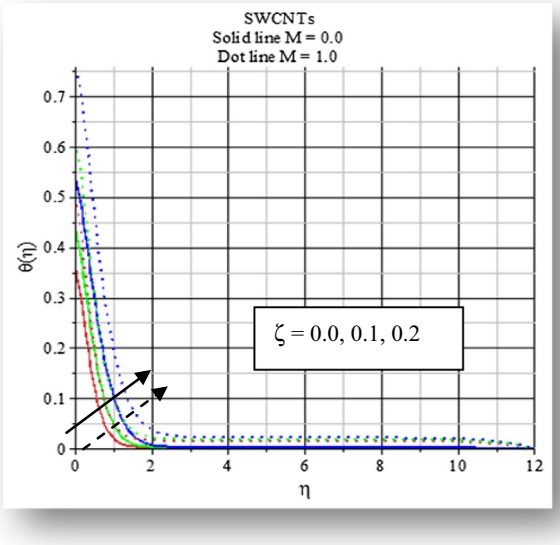

Figure 2 Comparison of temperature profile for ζ with Fig. 8(a) of Haq et al. [34].

4. Results and discussion

Eqs. (18) and (19) subjected to the boundary conditions (20) have been solved numerically for some values of the governing parameters Pr, ζ, m, λ, γ, n, n_1, λ_v and N using computer software MAPLE. The case $\gamma \gg 1.0$ corresponds to pure free convection, $\gamma = 1.0$ corresponds to mixed convection and $\gamma \ll 1.0$ corresponds to pure forced convection. Throughout this calculation we have considered $\gamma = 2.0$ unless otherwise specified. In order to validate our method, we have compared the results of $f''(0)$ with those of Haq et al. [34] and found them in excellent agreement, Table 2. Thus the present results are more accurate than their results.

It is also observed from Fig. 2 that the agreement with the theoretical solution of temperature profile for different values of nanoparticle volume fraction is correlated with Fig. 8(a) of Haq et al. [34].

Fig. 3 presents the characteristic temperature profiles for different values of the convective radiation parameter N in the presence of SWCNTs – water and Cu-water. According to Eqs. (2) and (3), the divergence of the radiative heat flux $\frac{\partial q''_{rad}}{\partial y}$ increases as thermal conductivity of the fluid (k_f) increases which in turn increases the rate of radiative heat transferred to the nanofluid (Cu-water) and hence the fluid temperature increases significantly as compared to that of SWCNTs-water. In view of this explanation, the effect of convective radiation becomes more significant as $N \to 0 (N \neq 0)$ and can be neglected when $N \to \infty$. It is noticed that the temperature of Cu – water increases significantly with increase of the radiation parameter N because of high thermal conductivity $\rho = 8933\ W/mK$ of the copper nanoparticles compared with SWCNTs $\rho = 2600\ W/mK$ while the rate of heat transfer decreases with increase of thermal radiation (Table 3) which is a good agreement of heat transfer mechanism. Further, it is also observed that the temperature of Cu-water is accelerated significantly as compared to the SWCNTs-water, which means that the Cu-water plays an important role in the cooling and heating processes.

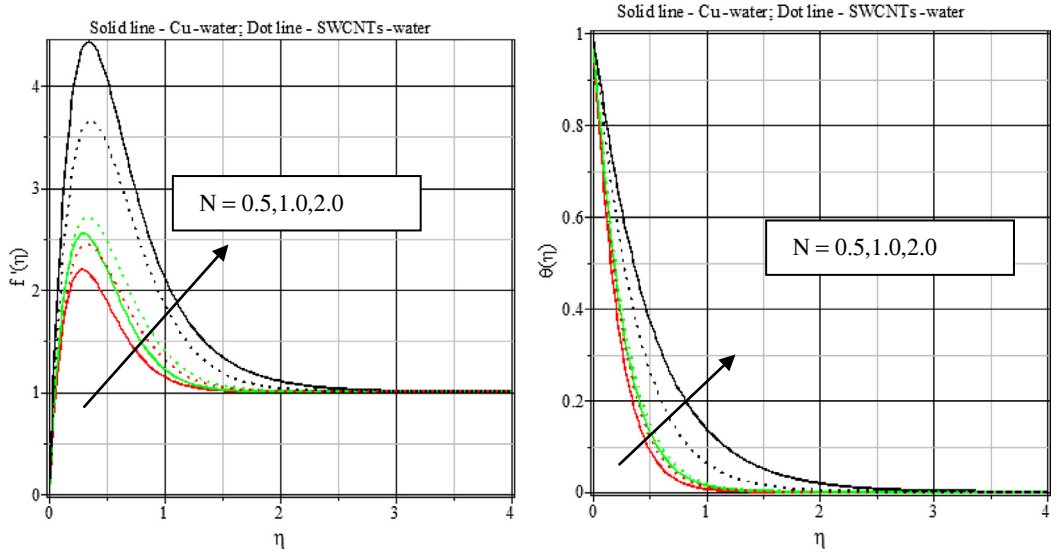

Figure 3 Thermal radiation effects on velocity and temperature profiles.

Table 3 $f''(0)$ and $-\theta'(0)$ for different values of N with $Pr = 6.2$, $\lambda = 0.5$, $n = 0.5$, $\delta = 0.5$, $\delta 1 = 1.0$, $M = 1.0$.

N	$f''(0)$	$-\theta'(0)$
Cu-water		
0.5	20.55279669098990	4.013066578174958
1.0	22.62423862620915	3.391590945118981
2.0	32.14574025942882	1.726288115317016
SWCNTs-water		
0.5	20.28956496528942	3.512247215249819
1.0	21.63920518519670	3.135233081911816
2.0	25.95668125217416	2.245444813624964

Table 4 $f''(0)$ and $-\theta'(0)$ for different values of M with $Pr = 6.2$, $\lambda = 0.5$, $n = 0.5$, $\delta = 0.5$, $\delta 1 = 1.0$, $N = 0.5$.

M	$f''(0)$	$-\theta'(0)$
Cu-water		
0.5	20.70162409209962	4.02508176167678
3.0	20.05149065422906	3.97100526599366
5.0	19.66480969147350	3.93644760221263
SWCNTs-water		
0.5	20.48272603838675	3.52727296683336
3.0	19.66075227457613	3.46120328554484
5.0	19.19520332503664	3.42074865447011

Fig. 4 presents the velocity and the temperature profiles for different values of magnetic parameter in the presence of water based SWCNTs and Cu nanoparticles. Due to the uniform thermal radiation, it is clearly shown that the abovementioned two cases, the velocity/temperature of water based SWCNTs and Cu-water decelerates/accelerates with increase of the strength of magnetic field, which implies that the applied magnetic field tends to heat the fluid and enhances the heat transfer from the wall. It is also observed that the momentum and the thermal boundary layer thickness for SWCNTs – water are significantly stronger than that of Cu-water because of the combined effects of electric and thermal conductivity of the SWCNTs-water Table 1. It indicates that the fluid temperature distribution is raised by decreasing the density of the water based SWCNTs and confirms the fact that the application of a magnetic field to an electrically conducting fluid produces a dragline force which causes acceleration in the nanofluid temperature. It is noticed from Table 4 that the rate of heat transfer increases with increase of magnetic strength, whereas the strength of rate of heat transfer for Cu-water is more significant compared to that of SWCNTs-water. These results clearly demonstrate that the combined effect of thermal radiation with magnetic field can be used as a means of controlling the flow and heat transfer characteristics because of the thermal conductivity of the water based SWCNTs.

Effects of heat source on velocity and the temperature distribution in the presence of water based SWCNTs and Cu-water are shown in Fig. 5. The term $Q_0(T_\infty - T)$ is assumed to be the amount of heat generated $(Q_0 > 0)$/absorbed $(Q_0 < 0)$ per unit volume. The presence of heat source in the boundary layer generates energy which causes the rate of heat transfer of the both nanofluids (water based SWCNTs and copper) to increase (Table 5), whereas the temperature of the nanofluids decreases (Fig. 5) with increase of heat source parameter, $\delta_1 > 0$. It is interesting to note that the thermal boundary layer thickness of the SWCNTs-water is higher than that of Cu-water because of high thermal conductivity of the SWCNTs, $k = 6600\ \mathrm{W}/m$. This decrease in temperature produces decrease in the flow field due to the buoyancy effect for SWCNTs-water and Cu-water. On the other hand, the presence of heat sink in the boundary layer absorbs energy which causes the rate of heat transfer of the nanofluids to opposite reaction. All these physical behaviors are the combined effects of thermal conductivity and diffusivity of the SWCNTs – water and Cu-water.

It is obtained that the rate of the nanofluids heat transfer decreases (Table 6), while velocity/temperature of SWCNTs – water and Cu-water increases/decreases with increase of nanoparticle volume fraction and tends asymptotically to zero as the distance increases from the boundary, Fig. 6. The sensi-

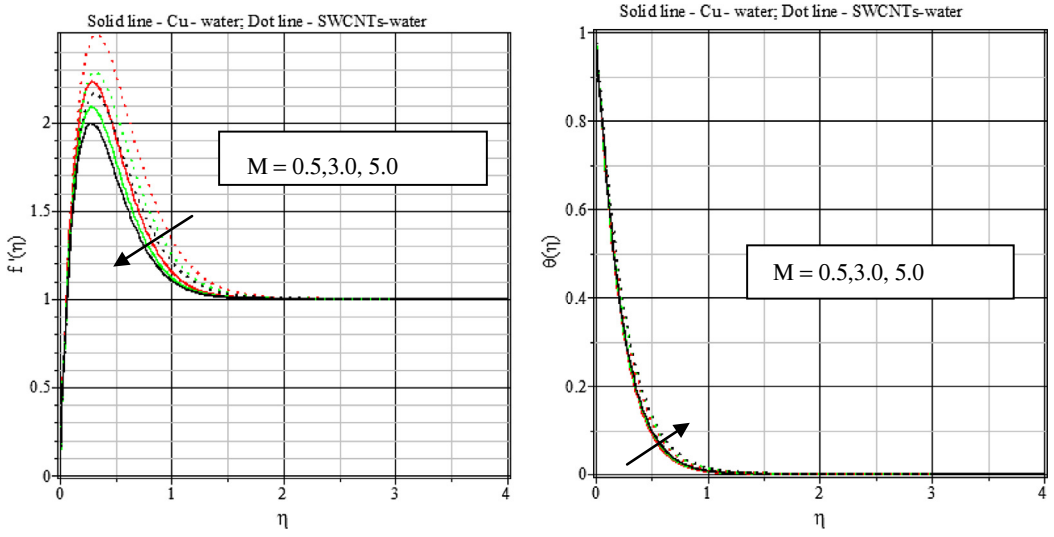

Figure 4 Magnetic effects on velocity and temperature profiles.

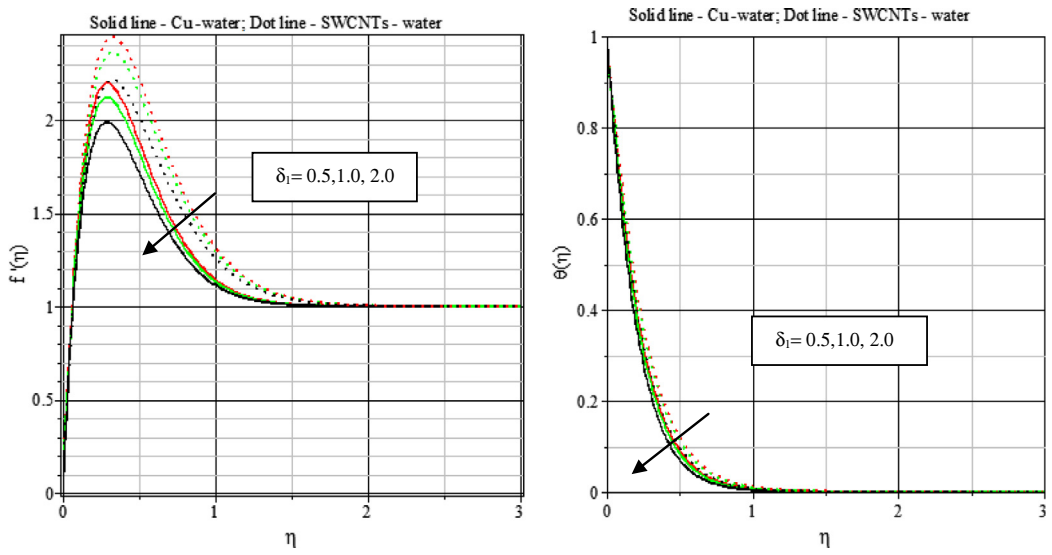

Figure 5 Heat source effects on velocity and temperature profiles.

Table 5 $f''(0)$ and $-\theta'(0)$ for different values of $\delta 1$ with $Pr = 6.2$, $\lambda = 0.5$, $n = 0.5$, $\delta = 0.5$, $M = 1.0$, $N = 0.5$.

$\delta 1$	$f''(0)$	$-\theta'(0)$
Cu-water		
0.5	20.55279643800090	4.01306655579183
1.0	20.05754457410864	4.23472337618584
2.0	19.17298696059175	4.65283631882094
SWCNTs-water		
0.5	20.28956072993407	3.51224680871207
1.0	19.82984126269601	3.70194211818746
2.0	18.99991077564455	4.06152427576732

Table 6 $f''(0)$ and $\theta'(0)$ for different values of ζ with $Pr = 6.2$, $\lambda = 0.5$, $n = 0.5$, $\delta 1 = 0.5$, $M = 1.0$, $N = 0.5$.

ζ	$f''(0)$	$-\theta'(0)$
Cu-water		
0.05	21.07726708958895	4.64854683528443
0.10	20.55279643800090	4.01306655579183
0.20	18.66649290351593	3.05707881048599
SWCNTs-water		
0.05	21.05119736138680	4.31425183415700
0.10	18.50274122814509	4.11882551922163
0.20	17.50574701225753	2.48235119953384

tivity of thermal boundary layer thickness with ζ is related to the increased thermal conductivity of the water based SWCNTs and Cu-water. It is also observed that the thermal boundary thickness of SWCNTs – water is higher than that of Cu-water because the high thermal conductivity of SWCNTs-water causes a drop in the temperature gradients and accordingly increases the thermal boundary thickness as demonstrated in Fig. 6. It is concluded that the size and shape of the SWCNTs in the presence of water play a dominant role on heat transfer mechanism.

The effects of nanoparticles in the based fluid (water) with $M = 1.0$ and $M = 2$ on the dimensionless velocity and temperature profiles have been displayed in Fig. 7. It is observed that the velocity and the temperature of the nanofluids firstly decrease and then increase (Fig. 7), whereas the rate of heat transfer firstly increases and then decreases (Table 7) with the increase of nanofluids in the following said sequences of water based Cu, Al_2O_3 and *SWCNTs*. It is observed that the thermal boundary layer thickness of SWCNTs – water for $M = 1.0$ is stronger than that of $M = 2.0$ and also the variation of the thermal diffusivity and conductivity of the SWCNTs-water within the boundary layer plays a dominant role compared to that of all the other nanofluids. It is noticed from Table 7 that the rate of heat transfer of SWCNTs is lower than that of all the other nanofluids because of thermal expansion and conductivity of the SWCNTs. The reason for this behavior is that the inertia of the porous medium and thermal conductivity of the nanofluid, SWCNTs – water provides an additional resistance to the nanofluid flow mechanism.

Fig. 8 presents the velocity and temperature profiles for different values of the thermal radiation parameter N in the presence of SWCNTs – seawater and SWCNTs-water. In the presence of uniform magnetic field, the comparison results between the thermal boundary layer thickness for SWCNTs-seawater and SWCNTs-water indicate that the SWCNTs-water is stronger than those of SWCNTs- seawater because of the combined effects of thermal conductivity and specific heat of water, Table 1. It is noticed that the velocity and temperature of the nanofluids (water and sea water based SWCNTs) increase, whereas the rate of heat transfer decreases with increase of thermal radiation. It is predicted that the rate of heat transfer of SWCNTs – seawater is stronger compared to that of SWCNTs-water significantly with increase of the radiation parameter N because of high density of sea water, Table 8. All the physical behaviors are the combined effects of thermal and electric conductivity of SWCNTs-seawater in the presence of magnetic field.

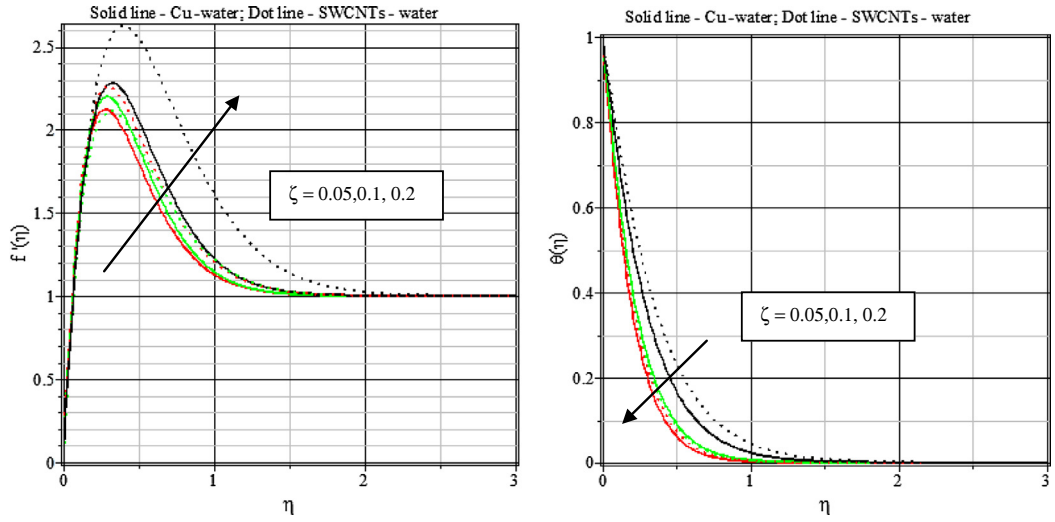

Figure 6 Nanoparticle volume fraction on velocity and temperature profiles.

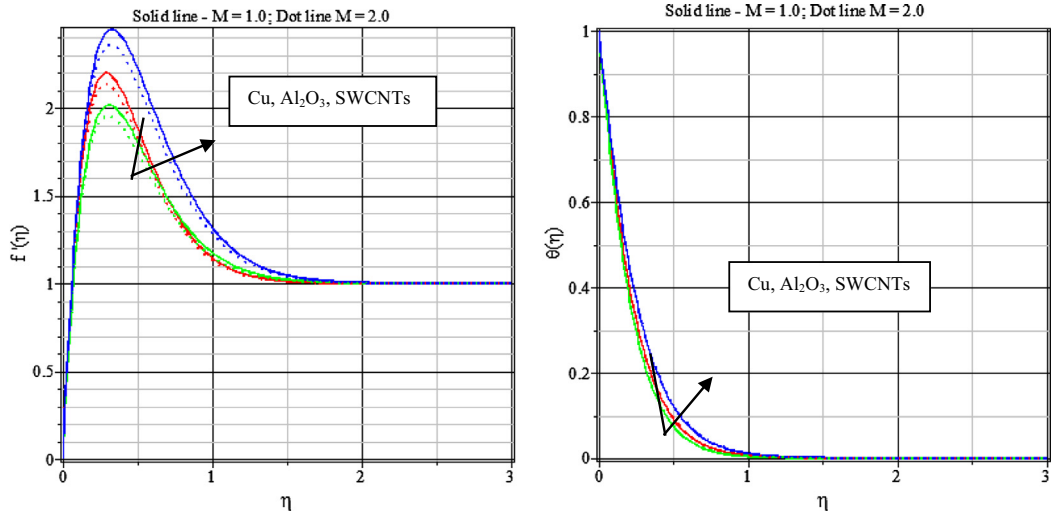

Figure 7 Different nanoparticles – water effects on velocity and temperature profiles.

Table 7 $f''(0)$ and $\theta'(0)$ for different nanoparticles with $Pr = 6.2$, $\lambda = 0.5$, $n = 0.5$, $\delta 1 = 0.5$, $N = 0.5$.

Nanoparticles	$f''(0)$	$-\theta'(0)$
$M = 1$		
Cu-water	20.552796438152647	4.013066555906404
Alumina-water	18.262401096460984	4.345462001444601
SWCNTs-water	20.289560729672772	3.512246808687515
$M = 2$		
Cu-water	20.285124889620853	3.990938830878775
Alumina-water	18.040860889891270	4.323075384252480
SWCNTs-water	19.949897955328400	3.485114876471530

5. Conclusions

Influence of the thermal radiation on MHD unsteady Hiemenz flow and heat transfer of incompressible (SWCNTs-water and Cu-water) nanofluid along a porous wedge sheet with variable stream conditions has been analyzed. It is worthwhile to provide the comparison among the base fluids in the presence of copper nanoparticles and single wall carbon nanotubes (SWCNT) for absolute skin friction and the rate of heat transfer. Moreover, the effects for various values of existing parameters are discussed for velocity and temperature. The main results of present analysis are listed below:

- The comparison results between SWCNTs-water and SWCNTs-seawater shows that the SWCNTs-seawater has the better performance to enhance convective heat transfer rate with increase of thermal radiation, whereas the thermal boundary layer thickness for SWCNTs-water is stronger than that of SWCNTs-seawater because of the thermal conductivity of water compared to that of seawater.
- The size and shape of the single walled carbon nanotubes play a dominant role on the temperature distribution. Physically, it is interesting to note that the momentum and thermal boundary layer thickness of the water based

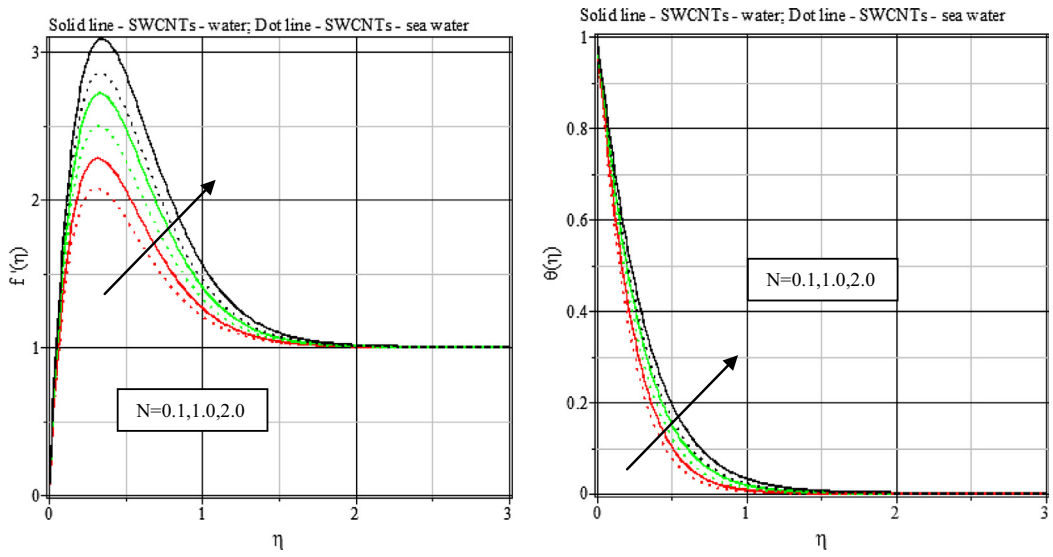

Figure 8 Thermal radiation effects on velocity and temperature profiles in the presence of SWCNTs-water and SWCNTs-seawater.

Table 8 $f'(0)$ and $-\theta'(0)$ for different values of N with $Pr = 6.2$, $\lambda = 0.5$, $n = 0.5$, $\delta = 0.5$, $\delta 1 = 1.0$, $M = 1.0$.

N	$f''(0)$	$-\theta'(0)$
SWCNTs-water		
0.1	19.39895848171915	3.797733214081592
1.0	21.63919164369924	3.135232033768488
2.0	23.40372709364394	2.722854871874763
SWCNTs-seawater		
0.1	18.42564684112256	4.251858901241890
1.0	20.68667639232926	3.481172497162533
2.0	22.46466065164271	3.009098578443907

SWCNTs are significantly stronger compared to those of the Cu-water with increase of nanoparticle volume fraction because the water based SWCNTs have high thermal conductivity.

- In the presence of uniform thermal radiation, the momentum and the thermal boundary layer thickness of SWCNTs-water are stronger than those of Cu-water with increase of magnetic field. It is clearly demonstrated that the combined effect of thermal radiation with magnetic field can be used as a means of controlling the flow and heat transfer characteristics because of the dynamic viscosity of the water based SWCNTs.
- The temperature of Cu-water increases significantly compared to that of SWCNTs-water with increase of the thermal radiation parameter. Thermal transport is significantly affected due to the thermal radiation of the nanofluids and it is more significant with different values of the parameters related to the SWCNTs-water as well as the Cu-water due to the thermal radiation energy.
- Increase of heat source in the boundary layer generates energy which causes the rate of heat transfer of the nanofluids (water based SWCNTs and copper) to increase whereas the rate of heat transfer of Cu-water is stronger than SWCNTs-water because of the density of copper nanoparticles compared to SWCNTs.
- The velocity and the temperature of the nanofluids firstly decrease and then increase whereas the rate of heat transfer firstly increases and then decreases with the increase of nanofluids in the following said sequences of water based Cu, Al_2O_3 and *SWCNTs*, which is a good agreement of heat transfer mechanism. In the presence of high strength of magnetic field, the temperature distribution of the SWCNTs-water within the boundary layer plays a dominant role compared to that of all the other nanofluids.

Seawater based single walled carbon nanotubes (SWCNTs-water) have attracted much attention because of their remarkable properties. Indeed, it was proved that the seawater based single walled carbon nanotubes have a high thermal and electrical conductivity properties. Among the usual nanoparticles, SWCNTS have attracted special interest due to unique thermal properties and structure. Therefore, CNTs can be a good option to disperse in the common working fluids to enhance the heat transfer and also the water based single walled carbon nanotubes are very prevalent in today's world of medical research.

Acknowledgment

The work was partly supported by Universiti Tun Hussein Onn Malaysia, Johor, Malaysia, under the Fundamental Research Grant Scheme No. 1208/2013.

References

[1] S. Choi, Enhancing thermal conductivity of fluids with nanoparticules, in: D.A. Siginer, H.P. Wang (Eds.), Developments Applications of Non-Newtonians Flows, vol. 66, American Society of Mechanical Engineers, 1995, pp. 99–105.
[2] Y. Li, J. Zhou, S. Tung, E. Schneider, S. Xi, A review on development of nanofluid preparation and characterization, Powder Tech. 196 (2009) 89–101.
[3] P. John, P.D. Shima, Thermal properties of nanofluids, Adv. Colloid Interf. Sci. 183 (2012) 30–45.

[4] W. Daungthongsuk, S. Wongwises, A critical review of convective heat transfer of nanofluids, Renew. Sust. Energy Rev. 11 (2007) 797–817.
[5] G. Huminic, A. Huminic, Application of nanofluids in heat exchangers: a review, Renew. Sust. Energy Rev. 16 (2012) 5625–5638.
[6] O. Mahian, A. Kianifar, S.A. Kalogirou, I. Pop, S. Wongwises, A review of the applications of nanofluids in solar energy, Int. J. Heat Mass Transfer 57 (2013) 582–594.
[7] G. Colangelo, E. Favale, A. de Risi, D. Laforgia, A new solution for reduced sedimentation flat panel solar thermal collector using nanofluids, Appl. Energy 111 (2013) 80–93.
[8] A.M. Hussein, K.V. Sharma, R.A. Bakar, K. Kadirgama, A review of forced convection heat transfer enhancement and hydrodynamic characteristics of a nanofluid, Renew. Sust. Energy Rev. 29 (2014) 734–743.
[9] C. Kleinstreuer, Y. Feng, Experimental and theoretical studies of nanofluid thermal conductivity enhancement: a review, Nanoscale Res. Lett. 6 (2011) 229–301.
[10] Sohail Nadeem, Rizwan Ul Haq, Zafar Hayat Khan, Heat transfer analysis of water-based nanofluid over an exponentially stretching sheet, Alexand. Eng. J. 53 (2014) 219–224.
[11] S.T. Hussain, Sohail Nadeem, Rizwan Ul Haq, Model based analysis of micropolar nanofluid flow over a stretching surface, Euro. Phys. J. Plus 129 (2014) 129–161.
[12] Rizwan Ul Haq, Zafar Hayat Khan, Waqar Ahmed Khan, Thermophysical effects of carbon nanotubes on MHD flow over a stretching surface, Phys. E: Low-Dimen. Syst. Nanostruct. 63 (2014) 215–222.
[13] S. Saleem, S. Nadeem, Rizwan Ul Haq, Buoyancy and metallic particle effects on an unsteady water-based fluid flow along a vertically rotating cone, Euro. Phys. J. Plus 129 (2014) 213.
[14] Rizwan Ul Haq, Zakia Hammouch, Waqar Ahmed Khan, Water-based squeezing flow in the presence of carbon nanotubes between two parallel disks, Therm. Sci. (2015), http://dx.doi.org/10.2298/TSCI141102148H.
[15] A. Waqar, I. Khan, I. Richard Culham, Rizwan Ul Haq, Heat transfer analysis of MHD water functionalized carbon nanotube flow over a static/moving wedge, J. Nanomater. 13 (2015), http://dx.doi.org/10.1155/2015/934367 934367.
[16] W.A. Khan, Z.H. Khan, R.U. Haq, Flow and heat transfer of ferrofluids over a flat plate with uniform heat flux, Euro. Phys. J. Plus 130 (2015) 86–91.
[17] Rizwan Ul Haq, S. Nadeem, Z.H. Khan, N.F.M. Noor, MHD squeezed flow of water functionalized metallic nanoparticles over a sensor surface, Phys. E: Low-Dimen. Syst. Nanostruct. 73 (2015) 45–53.
[18] A. Sharma, V.V. Tyagi, C.R. Chen, D. Buddhi, Review on thermal energy storage with phase change materials and applications, Ren. Sust. Energy Rev. 13 (2009) 318–345.
[19] A.J. Hunt, Small particle heat exchangers, Lawrence Berkeley Laboratory Report No.LBL-7841. J. Renew. Sust. Energy (1978).
[20] J. Buongiorno , W. Hu, Nanofluid coolants for advanced nuclear power plants, Paper no. 5705, in: Proceedings of ICAPP '05, Seoul, 2005, pp. 15–19.
[21] J. Buongiorno, Convective transport in nanofluids, ASME J. Heat Transfer 128 (2006) 240–250.
[22] A.V. Kuznetsov, D.A. Nield, Natural convective boundary-layer flow of a nanofluid past a vertical plate, Int. J. Therm. Sci. 49 (2010) 243–247.
[23] D.A. Nield, A.V. Kuznetsov, The Cheng–Minkowycz problem for natural convective boundary layer flow in a porous medium saturated by a nanofluid, Int. J. Heat Mass Transfer 52 (2009) 5792–5795.
[24] P. Cheng, W. Minkowycz, Free convection about a vertical flat plate embedded in a porous medium with application to heat transfer from a dike, J. Geophys. Res. 82 (1977) 2040–2044.
[25] Gaurav Lalwani, Andrea Trinward Kwaczala, Shruti Kanakia, Sunny C. Patel, Stefan Judex, Balaji Sitharaman, Fabrication and characterization of three-dimensional macroscopic all-carbon scaffolds, Carbon 53 (2013) 90–100.
[26] D.A. Nield, A.V. Kuznetsov, The Cheng–Minkowycz problem for natural convective boundary-layer flow in a porous medium saturated by a nanofluid, Int. J. Heat Mass Transfer 52 (2009) 5792–5795.
[27] A.V. Kuznetsov, D.A. Nield, Natural convective boundary-layer flow of a nanofluid past a vertical plate, Int. J. Therm. Sci. 49 (2010) 243–247.
[28] W.A. Khan, I. Pop, Boundary-layer flow of a nanofluid past a stretching sheet, Int. J. Heat Mass Transfer 53 (2010) 2477–2483.
[29] O.D. Makinde, A. Aziz, Boundary layer flow of a nanofluid past a stretching sheet with a convective boundary conditions, Int. J. Thermal Sci. 50 (2011) 1326–1332.
[30] S. Nadeem, C. Lee, Boundary layer flow of nanofluid over an exponentially stretching surface, Nanoscale Res. Lett. 94 (7) (2012) 1.
[31] W. Khan, Z. Khan, M. Rahi, Fluid flow and heat transfer of carbon nanotubes along a flat plate with Navier slip boundary, Appl. Nano Sci. 4 (2014) 633–641.
[32] N.G. Kafoussias, N.D. Nanousis, Magnetohydrodynamic laminar boundary layer flow over wedge with suction or injection, Canad. J. Phys. 75 (1997) 733–781.
[33] H. Schlichting, Boundary layer theory, McGraw Hill Inc., New York, 1979.
[34] Rizwan Ul Haq, Sohail Nadeem, Z.H. Khan, N.F.M. Noor, Convective heat transfer in MHD slip flow over a stretching surface in the presence of carbon nanotubes, Physica B 457 (2015) 40–47.
[35] Lynne D. Talley, George L. Pickard , William J. Emery, James H. Swift, Descriptive Physical Oceanography, Physical Properties of Sea Water, sixth ed., Elsevier Ltd, 2011, pp. 29–65, ISBN: 978-0-7506-4552-2 (Chapter 3).